

Gravitational Waves from Phase Transitions in Scale Invariant Models

Amine Ahriche¹ Shinya Kanemura² Masanori Tanaka²

¹*Department of Applied Physics and Astronomy, University of Sharjah, P.O. Box 27272 Sharjah, UAE.*

²*Department of Physics, Osaka University, Toyonaka, Osaka 560-0043, Japan.*

E-mail: ahriche@sharjah.ac.ae, kanemu@het.phys.sci.osaka-u.ac.jp,
m-tanaka@het.phys.sci.osaka-u.ac.jp

ABSTRACT: We investigate the properties of the gravitational waves (GW) generated during a strongly first order electroweak phase transition (EWPT) in models with the classical scale invariance (CSI). Here, we distinguish two parameter space regions that correspond to the cases of (1) light dilaton and (2) purely radiative Higgs mass (PRHM). In the CSI models, the dilaton mass, or the Higgs mass in the PRHM case, in addition to some triple scalar couplings are fully triggered by the radiative corrections (RCs). In order to probe the RCs effects on the EWPT strength and on the GW spectrum, we extend the standard model by a real singlet to assist the electroweak symmetry breaking and an additional scalar field Q with multiplicity N_Q and mass m_Q . After imposing all theoretical and experimental constraints, we show that a strongly first order EWPT with detectable GW spectra can be realized for the two cases of light dilaton and PRHM. We also show the corresponding values of the relative enhancement of the cross section for the di-Higgs production process, which is related to the triple Higgs boson coupling. We obtain the region in which the GW spectrum can be observed by different future experiments such as LISA and DECIGO. We also show that the scenarios (1) and (2) can be discriminated by future GW observations and measurements of the di-Higgs productions at future colliders.

Contents

1	Introduction	1
2	Models with Classical Scale Invariance	3
3	Constraints and Predictions	4
4	Gravitational Waves from a First Order Phase Transition	6
5	Numerical Results	8
6	Conclusion	14
A	Renormalization Group Equations	15

1 Introduction

The standard model (SM) in particle physics is a successful theory to explain results at the Large Hadron Collider (LHC) [1]. On the other hand, the SM has several experimental and theoretical problems. For the theoretical aspect, radiative corrections (RCs) to the Higgs boson mass cause the quadratic divergences in the SM, which is the origin of so-called the hierarchy problem [2]. Related to this problem, extended Higgs models with the classical scale invariance (CSI) have been often considered [3–16]. The CSI requires that all mass terms in the Lagrangian are forbidden. Therefore, the electroweak symmetry breaking (EWSB) does not occur at the tree-level. However, the CSI is violated by quantum effects of new particles. Then, the EWSB can be realized radiatively. This mechanism is often called as the Coleman-Weinberg mechanism [17]. An extension of the Coleman-Weinberg mechanism to the case with multi-scalar fields has been also discussed by Gildener and Weinberg [18]. The phenomenology of CSI extensions of the SM has been investigated in the literature, including the testability at current and future collider experiments [3–15].

Among the SM unsolved questions, the baryon asymmetry of the Universe is an important problem for both particle physics and cosmology. The observed baryon asymmetry is expressed by [19]

$$\eta_B = \frac{n_B - n_{\bar{B}}}{n_\gamma} = 6.143 \pm 0.190 \times 10^{-10}, \quad (1.1)$$

where n_B , $n_{\bar{B}}$ and n_γ refer to the number density of baryons, antibaryons and the CMB photons, respectively. In order to explain the ratio η_B , three conditions need to be satisfied simultaneously at the early Universe, known as the Sakharov conditions [20]. These conditions can be summarized by the existence of such interactions that violate the baryon number, violate C and CP symmetries; and occur out of the thermal equilibrium. One of the most interesting scenarios for baryogenesis is the electroweak baryogenesis (EWB), where the third Sakharov condition is satisfied via a strongly first order phase transition at the electroweak scale [21]. However, it has been shown that this scenario cannot be realized in the SM since the CP violation source in Yukawa interactions is too small to produce η_B and the electroweak phase transition (EWPT) is not first order. Therefore, going beyond the SM is mandatory. In order to realize the EWB

scenario, the sphaleron processes should decouple after the first order EWPT. This condition can be approximately expressed by [22–26]

$$\frac{v_c}{T_c} > 1, \quad (1.2)$$

where T_c is the critical temperature at which the potential minima (the false and true ones) are degenerate; and v_c is the vacuum expectation value (VEV) of the $SU(2)_L$ doublet scalar field at $T = T_c$. Once the condition (1.2) is satisfied, the triple Higgs boson coupling hhh significantly deviates from the SM prediction [27]. Therefore, precise measurements of the hhh coupling at future colliders are important to test the scenario of the EWB. In order to realize a large deviation in the triple Higgs boson coupling, large quantum corrections from new particles play an important role. Such large quantum corrections may be able to appear in the other Higgs boson couplings like $h\gamma\gamma$ [28–35].

In addition to the hhh coupling measurement, gravitational waves (GWs) generated during a strongly first order EWPT can be used to explore new physics models [36–39]. A first order phase transition at the early Universe occurs via the nucleation and expansion of bubbles of the broken vacuum. When the broken vacuum bubbles collide with each other, detectable GWs can be produced. For a first order EWPT, the typical peak frequency of the GW spectrum is around $10^{-3} - 10^{-1}$ Hz [40]. Such GW spectrum can be observed by future space-based interferometers like LISA [41] and DECIGO [42]. It means that new physics models can be explored by using the GWs. Predictions on the GW spectrum in extended Higgs models with the CSI have been discussed in the literature [8, 43–50]. The dynamics of the EWPT in the CSI models has been also discussed in the literature [8, 51–55].

Recently, it is often discussed that the first order EWPT can be tested by primordial black hole observations [56, 57]. When the first order EWPT forms primordial black holes (PBHs), those masses are around 10^{-5} times of the solar mass. It implies that we can test the first order EWPT by observing such PBHs at current and future microlensing experiments like Subaru HSC [58], OGLE [59], PRIME [60] and Roman telescope [61].

The CSI implies that a CP-even scalar should be massless at tree-level; and becomes massive due to the quantum corrections that trigger the EWSB. In Ref. [14], a generic model has been considered to investigate the RC effects on the EWSB, dilaton mass, scalar mixing, as well other observables. In this model, the SM is extended by a real singlet and an extra singlet Q with multiplicity N_Q and the couplings (α_Q, β_Q) to the Higgs doublet and real singlet, respectively. Then, the RCs are quantified by using N_Q, α_Q and β_Q in addition to the singlet VEV. In a case of large (N_Q, α_Q, β_Q) , the dilaton mass can be 125 GeV due to the large RCs. This scenario corresponds to the case of a purely radiative Higgs mass (PRHM) [14]. Although large RCs (with large values for N_Q, α_Q , and β_Q) are beneficial for vacuum stability, they may introduce tension with the triviality bound [62, 63]. This aspect needs to be investigated within the viable parameter space of this model.

In this work, we will investigate the effect of quantum corrections on the EWPT dynamics and on the corresponding GW spectrum using this generic CSI model with a scalar mixing [14]. Here, the triple scalar couplings are very sensitive to the quantum corrections, which makes the di-Higgs production cross section at both LHC and ILC useful observables to probe the viable parameter space. According to the full LHC Run 2 data with 139 fb^{-1} , it is required that the cross section for the non-resonant di-Higgs production process is lower than 3.4 times of the SM prediction [64]. At the High Luminosity LHC (HL-LHC), the cross section will be measured by 0.7 times of the SM prediction [64, 65]. At the International Linear Collider (ILC), it is expected that the di-Higgs production cross section is limited less than 2 or 3 times of the SM prediction [66]. The di-Higgs production processes in extended Higgs models have been investigated in the literatures [67–74]. In this paper, we show that the light dilaton and PRHM

cases can be distinguished by using complementarity between collider experiments and GW observations.

The structure of this paper is as follows. In Section 2, we introduce the CSI models; and discuss the EWSB and the scalar mass spectrum. In Section 3, we identify the theoretical and experimental constraints on these CSI models. In Section 4, we define the parameters characterizing the first order EWPT and the corresponding GW spectrum. Our numerical results for GW observations and collider experiments are shown in Section 5. Our conclusion is given in Section 6.

2 Models with Classical Scale Invariance

The CSI in quantum field theories is defined by $x^\mu \rightarrow \kappa^{-1}x^\mu$, $\psi_i \rightarrow \kappa^a\psi_i$ with $a = 1, 3/2$ for bosons and fermions, respectively. This invariance implies that the scalar quadratic terms vanish. Therefore, the general representation of the potential with the CSI is given by [18]

$$V(\Phi_i) = \sum_{i,j,k,l} \lambda_{ijkl} \Phi_i \Phi_j \Phi_k \Phi_l, \quad (2.1)$$

where Φ_i represents all the scalar representations. Obviously, the EWSB could not take place because the scalar potential in Eq. (2.1) contains only quartic terms, which requires the contributions of the quantum corrections that break both of the electroweak and CSI symmetries at the same time. In order to achieve the EWSB in this class of models, the SM is extended by a real singlet S ; in addition to other bosonic and fermionic degrees of freedom (dof) with (n_i, α_i, β_i) as multiplicities and couplings to the Higgs doublet and scalar S , respectively. Here, the Higgs doublet field \mathcal{H} and the singlet field S are written as

$$\mathcal{H} = \begin{pmatrix} \chi^+ \\ \frac{H+i\chi^0}{\sqrt{2}} \end{pmatrix}, \quad S = s, \quad (2.2)$$

with χ^+ and χ^0 are the Goldstones; and $\langle H \rangle = v$ and $\langle s \rangle = v_S$ are the VEV of the doublet and singlet, respectively. In this model, two CP-even eigenstates $h_{1,2}$ (with $m_2 > m_1$) are obtained by using the 2×2 mixing matrix with angle α . We distinguish two possibilities where the observed SM-like Higgs with the mass $m_h = 125$ GeV corresponds to (1) $h_2 \equiv h$ and $h_1 \equiv \eta$ is a light dilaton (light dilaton scenario); and (2) $h_1 \equiv h$ and $h_2 \equiv \eta$ is a heavy scalar (PRHM scenario) [14].

The full one-loop effective potential in terms of CP-even fields (H, s) can be written as

$$V^{1\ell}(H, s) = \frac{1}{24}(\lambda_H + \delta\lambda_H)H^4 + \frac{1}{24}(\lambda_S + \delta\lambda_S)s^4 + \frac{1}{4}(\omega + \delta\omega)H^2s^2 + \sum_i n_i G(m_i^2(H, s)), \quad (2.3)$$

with $\delta\lambda_H, \delta\lambda_S, \delta\omega$ are the counter terms, n_i and $m_i^2(H, s)$ are the multiplicities and the field dependent masses for particles running loops, respectively. Here, the function $G(r)$ is defined a la \overline{DR} scheme, i.e., $G(r) = \frac{r^2}{64\pi^2}(\log(r/\Lambda^2) - 3/2)$, with the renormalization scale is taken to be $\Lambda = m_h = 125.18$ GeV.

In this setup, we can eliminate the couplings λ_H, λ_S and ω in favor of the tadpole conditions and the Higgs mass at tree-level, and the corresponding counter-terms $\delta\lambda_H, \delta\lambda_S, \delta\omega$ can be also eliminated using the one-loop tadpole and Higgs mass conditions as shown in Refs. [14, 15]. In case where all field dependent masses can be written in the form¹ $m_i^2(H, s) = \frac{1}{2}(\alpha_i H^2 + \beta_i s^2)$,

¹Indeed, all field dependent masses can be written in this form except the eigenmasses of $h_{1,2}$. The contributions of $h_{1,2}$ to the effective potential can be safely neglected.

the counter-terms can be simplified as

$$\delta\omega = \frac{m_h^2}{v^2 + v_S^2} \frac{(ab - c^2)(v^2 + v_S^2) - av_S^2 - bv^2 + 2cvv_S}{av^2 + bv_S^2 + 2cvv_S - v^2 - v_S^2}, \quad (2.4)$$

with

$$\begin{aligned} a &= \frac{1}{32\pi^2 m_h^2} \sum_i n_i \alpha_i \left(2m_i^2 - \beta_i v_S^2 \log \frac{m_i^2}{\Lambda^2} \right), \\ b &= \frac{1}{32\pi^2 m_h^2} \sum_i n_i \beta_i \left(2m_i^2 - \alpha_i v^2 \log \frac{m_i^2}{\Lambda^2} \right), \\ c &= \frac{vv_S}{32\pi^2 m_h^2} \sum_i n_i \alpha_i \beta_i \log \frac{m_i^2}{\Lambda^2}. \end{aligned}$$

The light dilaton and PRHM cases are identified via the conditions [14, 15]

$$\delta\omega(v^2 + v_S^2)/m_h^2 < a + b < 1 + \delta\omega(v^2 + v_S^2)/m_h^2 \quad (\text{for light dilaton case}), \quad (2.5)$$

$$a + b > 1 + \delta\omega(v^2 + v_S^2)/m_h^2 \quad (\text{for PRHM case}), \quad (2.6)$$

respectively. However, the condition $a + b = 1 + \delta\omega(v^2 + v_S^2)/m_h^2$ corresponds to the special case of degenerate eigenmasses $m_1 = m_2 = m_h$. This case is of great interest that deserves an independent study.

In our analysis, we consider a generic model where the SM is extended by a scalar singlet S to assist the EWSB; and another boson Q with multiplicity N_Q and the squared mass $m_Q^2 = \frac{1}{2}(\alpha_Q v^2 + \beta_Q v_S^2)$. Clearly, the quantum correction from the boson Q is proportional to the field multiplicity N_Q , the couplings (α_Q, β_Q) to \mathcal{H} and S and/or the singlet VEV v_S .

3 Constraints and Predictions

The different constraints on this model have been discussed in details in Ref. [14]. Here, we mention the constraints coming from the total Higgs strength modifier $\mu_{\text{tot}} = c_\alpha^2 \times (1 - \mathcal{B}_{BSM}) \geq 0.89$ at 95 % CL [75], that implies the scalar mixing to be $s_\alpha^2 \leq 0.11$ in the absence of invisible and undetermined Higgs decay ($\mathcal{B}_{BSM} = 0$). Here, the RCs play a crucial role to satisfy this bound. The mixing sine can be decomposed into a tree-level part and a one-loop part as $s_\alpha = s_\alpha^{(0)} + s_\alpha^{(1)}$, where $s_\alpha^{(0)} = v/\sqrt{v^2 + v_S^2}$ in the light dilaton case. Therefore, small RCs will keep the constraint $s_\alpha^2 \leq 0.11$ fulfilled for $v_S \gg v$. However, in the PRHM case, we have $s_\alpha^{(0)} = v_S/\sqrt{v^2 + v_S^2}$ which makes the constraint $s_\alpha^2 \leq 0.11$ explicitly violated for $v_S \gg v$. Interestingly, large RCs in the PRHM case that are responsible to push the light CP-even eigenmass from zero tree-level value to the measured 125 GeV; are also responsible to generate large negative contributions to the mixing $s_\alpha^{(1)}$ that makes the condition $s_\alpha^2 \leq 0.11$ fulfilled. This point has been discussed in details in Ref. [14] for this model; and in Ref. [15] for the SI scotogenic model.

The counter-terms $\delta\lambda_H$, $\delta\lambda_S$, $\delta\omega$ cannot take any numerical values since they are constrained by the one-loop perturbativity conditions $\lambda_H^{1-\ell}$, $\lambda_S^{1-\ell}$, $|\omega^{1-\ell}| < 4\pi$. Here, the one-loop quartic couplings are defined as the 4th derivatives of the full one-loop scalar potential in Eq. (2.3) at the broken vacuum. In what follows, we will consider the one-loop value for the Higgs-dilaton mixing angle, since it has been shown that the role of RCs is crucial in driving the mixing value towards the experimentally allowed region, both in the context of a light dilaton and PRHM cases [14]. In the CSI models, the leading term in the one-loop scalar potential is $\varphi^4 \log \varphi$ rather than φ^4 , where φ could be any direction in the H - s plane. Thus, the vacuum stability conditions differ from those used in the literature, which are given by $\sum_i n_i \alpha_i^2 > 0 \wedge \sum_i n_i \beta_i^2 > 0$ [14, 15].

In addition to the perturbativity and vacuum stability conditions, we discuss here the triviality bound as a theoretical constraint on our model. The triviality bound plays a significant role in discussing upper bounds on couplings [76]. Especially, the triviality bound can give strong constraints on models with the CSI or a strongly first order EWPT [62, 63]. Generally, the Landau pole scale is defined as the energy scale at which the perturbative description of the model is broken down, which suggests the need for a more fundamental theory or modifications at higher energy scales. In this work, we define the Landau pole scale (Λ_{Lan}) as the approximate scale where $\Lambda_{\text{Lan}} = \min(\{\Lambda_i\})$ with $\lambda_i(\mu = \Lambda_i) = 4\pi$, and $\lambda_i(\mu)$'s are the couplings at the scale μ in our model. In what follow, we consider the condition $\Lambda_{\text{Lan}} < 10$ TeV as a triviality bound.

In Appendix A, we present the β -functions for the renormalization group equations (RGEs) in our model using the ordinary scheme. However, these functions do not decouple the effects of heavy new particles in the RGEs flow, even when our focus is on physics at a low energy scale. These non-decoupling effects are commonly known as threshold effects. Recently, it has been confirmed that such threshold effects can be naturally taken into account by employing mass-dependent β -functions [77]. In the following, we will utilize the mass-dependent β -function when discussing the RGEs analysis.

As well known, the triple Higgs boson coupling, $\lambda_{hhh} = \lambda_{hhh}^{\text{SM}}(1 + \Delta_{hhh})$, is an important quantity to probe the strongly first order EWPT [27, 78, 79]. In order to obtain information about the relative triple Higgs coupling enhancement (Δ_{hhh}), it is necessary to measure the di-Higgs production processes at the LHC or the ILC. However, in models where the SM Higgs doublet mixes with a singlet, as in our model, the di-Higgs production process involves an extra Feynman triangle diagram mediated by the extra scalar η . In this case, the di-Higgs production cross section has three independent contributions that come from: (1) the Feynman diagrams involving only the triple scalar couplings λ_{hhh} and $\lambda_{hh\eta}$ (σ_λ), (2) the diagrams with only pure gauge couplings (σ_G); and (3) the interference contribution ($\sigma_{G\lambda}$) [14, 80]. In our model, the di-Higgs production cross section scaled by its SM value can be expressed as

$$R(hh + X) = \frac{\sigma(hh + X)}{\sigma_{\text{SM}}(hh + X)} = \frac{\xi_1 \sigma_G + \xi_2 \sigma_\lambda + \xi_3 \sigma_{G\lambda}}{\sigma_G + \sigma_\lambda + \sigma_{G\lambda}}. \quad (3.1)$$

The coefficients ξ_i ($i = 1, 2, 3$) are defined at the CM energy \sqrt{s} as [14, 80]

$$\xi_1 = c_\alpha^4, \quad \xi_2 = |\mathcal{P}|^2, \quad \xi_3 = c_\alpha^2 \Re(\mathcal{P}), \quad (3.2)$$

with

$$\mathcal{P} = c_\alpha \frac{\lambda_{hhh}}{\lambda_{hhh}^{\text{SM}}} + s_\alpha \frac{\lambda_{hh\eta}}{\lambda_{hhh}^{\text{SM}}} \frac{s - m_h^2 + im_h \Gamma_h}{s - m_\eta^2 + im_\eta \Gamma_\eta}, \quad (3.3)$$

where Γ_h is the measured Higgs total decay width, Γ_η is the estimated heavy scalar total decay width; and $\lambda_{hhh}^{\text{SM}}$ is the triple Higgs boson coupling in the SM. We take the value of $\lambda_{hhh}^{\text{SM}}$ as in Refs. [29, 30].

Here, we consider the di-Higgs production processes $pp \rightarrow hh$ and $e^+e^- \rightarrow Zhh$ at the LHC with 14 TeV and ILC with 500 GeV, respectively. In the following, we use the notations R_{LHC} and R_{ILC} for the processes $R(pp \rightarrow hh @ \text{LHC} 14 \text{ TeV})$ and $R(e^+e^- \rightarrow Zhh @ \text{ILC} 500 \text{ GeV})$, respectively. The values σ_λ , σ_G and $\sigma_{G\lambda}$ for the process $pp \rightarrow hh @ \text{LHC} 14 \text{ TeV}$ and $e^+e^- \rightarrow Zhh @ \text{ILC} 500 \text{ GeV}$ are given in Table. 1.

One has to notice that, in the PRHM scenario, the heavy scalar η decays into all SM Higgs final states in addition to a di-Higgs channel. This means that the negative searches for a heavy resonance at both ATLAS and CMS can be used to constraint our model, like: (1) the heavy CP-even resonance in the channels of pair of leptons, jets or gauge bosons $pp \rightarrow H \rightarrow \ell\ell, jj, VV$ [82–84]; and (2) the resonance in the di-Higgs production $pp \rightarrow H \rightarrow hh$ [85–87]. It has been shown in Ref. [14] that almost the full parameter space region is allowed even if we consider the heavy CP-even resonance. Thus, these constraints will not be considered in our work.

	σ_λ [fb]	σ_G [fb]	$\sigma_{G\lambda}$ [fb]	Reference
$pp \rightarrow hh$ @LHC 14TeV	70.1	9.66	-49.9	[81]
$e^+e^- \rightarrow Zhh$ @ILC 500GeV	0.0837	0.01565	0.05685	[14]

Table 1. The cross section contributions in Eq. (3.1) for each di-Higgs production process at the LHC and the ILC.

4 Gravitational Waves from a First Order Phase Transition

In order to analyze the GW spectrum generated during a strongly first order EWPT, we need to define the parameters α and β , which characterize the GWs from the dynamics of vacuum bubbles [40]. These parameters represent the latent heat and the inverse of the EWPT time duration, respectively. However, an accurate description of the EWPT dynamics is mandatory, which requires the exact knowledge of a key physical quantity: the full one-loop effective potential at finite temperature², that is given by [91]

$$V_{\text{eff}}^T(H, s, T) = V^{1\ell}(H, s) + T^4 \sum_{i=\text{all}} n_i J_{B,F}(m_i^2/T^2) + V_{\text{daisy}}(H, s, T), \quad (4.1)$$

$$J_{B,F}(\alpha) = \frac{1}{2\pi^2} \int_0^\infty dr r^2 \log \left[1 \mp \exp(-\sqrt{r^2 + \alpha}) \right], \quad (4.2)$$

where the last contribution in Eq. (4.1), that is called the daisy (or ring) part, represents the leading term of higher order thermal corrections [92]. This contribution can be taken into account by replacing the scalar and longitudinal gauge field-dependent masses in the first and second terms of Eq. (4.1) by their thermally corrected values, i.e., $m_i^2 \rightarrow \tilde{m}_i^2 = m_i^2 + \Pi_i$ [93]. The thermal self-energies are given by [94]

$$\begin{aligned} \Pi_H = \Pi_\chi &= T^2 \left(\frac{1}{2}\lambda_H + \frac{3}{16}g^2 + \frac{1}{16}g'^2 + \frac{1}{4}y_t^2 + \frac{\omega}{24} + \frac{\alpha_Q N_Q}{24} \right), \\ \Pi_S &= \left(\frac{\omega}{6} + \frac{\lambda_S}{24} + \frac{\beta_Q N_Q}{24} \right) T^2, \\ \Pi_Q &= T^2 \left(\frac{\alpha_Q}{4} + \frac{\beta_Q}{12} + \frac{\lambda_Q N_Q}{24} \right), \\ \Pi_{W_L} &= \frac{11}{6}g^2 T^2, \quad \Pi_{B_L} = \frac{11}{6}g'^2 T^2, \quad \Pi_{W_L, B_L} \simeq 0, \end{aligned} \quad (4.3)$$

with g and g' are the $SU(2)_L$ and $U(1)_Y$ gauge couplings, respectively. Here, λ_Q is the self-coupling constant of boson Q . Since the thermal corrections related to λ_Q only come from the thermal mass of the new boson Q , this correction can be negligible. Thus, for reasons of simplicity, we take $\lambda_Q = 0$ in our analysis.

The EWSB takes place during the transition from the symmetric vacuum ($\langle H \rangle = 0$) to the broken one ($\langle H \rangle \neq 0$), at the nucleation temperature $T_n \leq T_c$. A strongly first order EWPT occurs through the tunneling between the symmetric and broken vacuum, which corresponds to the vacuum bubble nucleation at random points in the space. These bubbles expand and collide with each other until filling the Universe by the broken vacuum ($\langle H \rangle \neq 0$). When a bubble wall passes through an unbroken symmetry region (where $\langle H \rangle = 0$) at which a net baryon asymmetry is generated by the $B + L$ and CP violating processes, the thermal equilibrium will washout this asymmetry unless the B number violating process is suppressed inside the bubble (broken vacuum $\langle H \rangle \neq 0$). This condition is often called as the sphaleron decoupling

²Recently, there has been a discussion on methods to decrease the uncertainty associated with the thermal effective potential, considering factors such as renormalization scale and gauge dependencies [88–90].

condition and approximately expressed by Eq. (1.2). It has been shown that the singlet plays an important role in the EWPT dynamics even though its VEV $\langle S \rangle_c$ is absent in the condition in Eq. (1.2) [23, 24]. The precise evaluation of the sphaleron decoupling condition in extended Higgs models has been also discussed in Refs. [25, 26].

In what follows, we analyze the GW spectrum from a first order EWPT in this model by estimating the above mentioned parameters α and β [40]. The parameter α is the latent heat normalized by the radiation energy density, which is given by

$$\alpha = \frac{\epsilon(T_n)}{\rho_{\text{rad}}(T_n)}, \quad (4.4)$$

with $\rho_{\text{rad}}(T) = (\pi^2/30)g_*T^4$ is the radiation energy density, g_* is relativistic degrees of freedom in the thermal plasma; and

$$\epsilon(T) = -V_{\text{eff}}^T(H(T), s(T), T) + T \frac{\partial V_{\text{eff}}^T(H(T), s(T), T)}{\partial T}, \quad (4.5)$$

is the released energy density, where the configuration $(H(T), s(T))$ is the broken vacuum at temperature T .

The parameter β that describes approximately the inverse of time duration of the EWPT is defined as

$$\beta = - \left. \frac{dS_E}{dt} \right|_{t=t_n} \simeq \left. \frac{1}{\Gamma} \frac{d\Gamma}{dt} \right|_{t=t_n}, \quad (4.6)$$

where S_E and Γ are the 4d Euclidean action of a critical bubble and vacuum bubble nucleation rate per unit volume per unit time at the time of the EWPT t_n , respectively. In the following, we use the normalized parameter β by Hubble parameter H_T

$$\tilde{\beta} = \frac{\beta}{H_T} = T_n \left. \frac{d}{dT} \left(\frac{S_3(T)}{T} \right) \right|_{T=T_n}, \quad (4.7)$$

where $S_3(T)$ is the 3d action for the bounce solution. The transition temperature T_n is defined by

$$\left. \frac{\Gamma}{H_T^4} \right|_{T=T_n} = 1, \quad (4.8)$$

with the bubble nucleation rate [95]

$$\Gamma(T) \simeq T^4 \left(\frac{S_3(T)}{2\pi T} \right)^{3/2} \exp \left[-\frac{S_3(T)}{T} \right]. \quad (4.9)$$

If Γ/H_T^4 cannot be larger than the unity ($\Gamma/H_T^4 \ll 1$), the first order phase transition does not complete by today. Thus, this condition is used as another theoretical constraint on our model. Here, we use the public code `CosmoTransitions` to obtain the bounce solutions [96].

The GWs from a first order phase transition can be produced via three mechanisms: (1) collisions of bubble walls and shocks in the plasma $\Omega_\phi h^2$ [39], (2) the compressional waves (sound waves) $\Omega_{\text{sw}} h^2$ [97]; and (3) magnetohydrodynamic (MHD) turbulence in the plasma $\Omega_{\text{tur}} h^2$ [98]. Therefore, the stochastic GW background can be approximately expressed by

$$\Omega_{\text{GW}} h^2 \simeq \Omega_\phi h^2 + \Omega_{\text{sw}} h^2 + \Omega_{\text{tur}} h^2. \quad (4.10)$$

The importance of each contribution depends on the EWPT dynamics, especially on the bubble wall velocity v_b . In this work, we take $v_b = 0.95$ as a free parameter; and focus on the contribution to GWs from the sound waves in the plasma, which is the dominant contributions

among the other GW sources. According to the numerical simulations, a fitting function for the GW spectrum from the sound waves is given by [99]

$$\Omega_{\text{sw}}(f)h^2 = \tilde{\Omega}_{\text{sw}}h^2 \times (f/\tilde{f}_{\text{sw}})^3 \left(\frac{7}{4 + 3(f/\tilde{f}_{\text{sw}})^2} \right)^{7/2}, \quad (4.11)$$

where the peak of the amplitude is given by

$$\tilde{\Omega}_{\text{sw}}h^2 \simeq 2.65 \times 10^{-6} v_b \tilde{\beta}^{-1} \left(\frac{\kappa\alpha}{1+\alpha} \right)^2 \left(\frac{100}{g_*} \right)^{1/3}; \quad (4.12)$$

and the peak frequency is expressed as

$$\tilde{f}_{\text{sw}} \simeq 1.9 \times 10^{-5} \text{Hz} \frac{1}{v_b} \tilde{\beta} \left(\frac{T_n}{100 \text{GeV}} \right) \left(\frac{g_*}{100} \right)^{1/6}, \quad (4.13)$$

with κ is the efficiency factor which characterize how much of the vacuum energy is converted into the fluid motion [100].

5 Numerical Results

In our analysis, we consider the following values for the multiplicity $N_Q = 6, 12, 24$; and the singlet VEV $v_S = 500 \text{ GeV}, 1 \text{ TeV}, 3 \text{ TeV}$, while allowing the couplings to lie within the perturbative regime $|\alpha_Q|, |\beta_Q| \leq 4\pi$. In addition, we consider the constraints: (1) vacuum stability, (2) the mixing angle $s_\alpha^2 \leq 0.11$, (3) the perturbativity one-loop constraints $\lambda_{H,S}^{1-\ell}, |\omega^{1-\ell}| < 4\pi$; and (4) the completion condition of the phase transition. As well known, the GWs from a first order EWPT is useful to probe the structure of the Higgs potential [8, 43]. Since the RCs have the key role in this model, one expects that future space-based interferometers would be able to detect the GWs generated during the first order EWPT. In order to understand the impact on the EWPT strength from the quantum corrections, we show the ratio v_c/T_c in the palette in Fig. 1 for different values of (α_Q, β_Q) , N_Q and v_S .

In all panels of Fig. 1, the upper parameter space region corresponds to the PRHM scenario; and the lower region is the light dilaton case. The regions colored in cyan represent the parameter region where the GW spectra from the first order EWPT may be detected at DECIGO [42]. Here, one notices that not only the dilaton case, but also the PRHM scenario predicts testable GW spectra. The magenta region in Fig. 1 is constrained by the completion condition of the first order EWPT. Interestingly, in Fig. 1, there is a parameter space region where the GW spectra can be tested at future space-based interferometers even if the EWPT is not strongly first order, i.e., the condition in Eq. (1.2) is not satisfied. One remarks that satisfying the condition in Eq. (1.2) requires small α_Q and β_Q . Furthermore, the triviality bound ($\Lambda_{\text{Lan}} < 10 \text{ TeV}$) excludes a portion of the parameter space corresponding to large values of α_Q and β_Q in the PRHM case. This observation has also been noted in extended scalar sector models, where more parameter space is excluded when the triviality bound is considered at a higher scale [101, 102]. On the other hand, as we will explain later, the di-Higgs production cross section can be large for relatively large β_Q value. It indicates a complementarity between the GW observations and collider experiments to test our model. The details for the di-Higgs production will be discussed later.

According to Fig. 1, as N_Q is getting large, the parameter space region satisfying the condition in (1.2) becomes large in the PRHM scenario. Whereas, in the light dilaton case, such parameter space region is narrowed down, which means that the PRHM scenario is preferred in order to realize the EWBG scenario within CSI models. From the results in Fig. 1, one learns that the scenario with degenerate masses $m_1 = m_2 = m_h$ is possible; and it corresponds to the

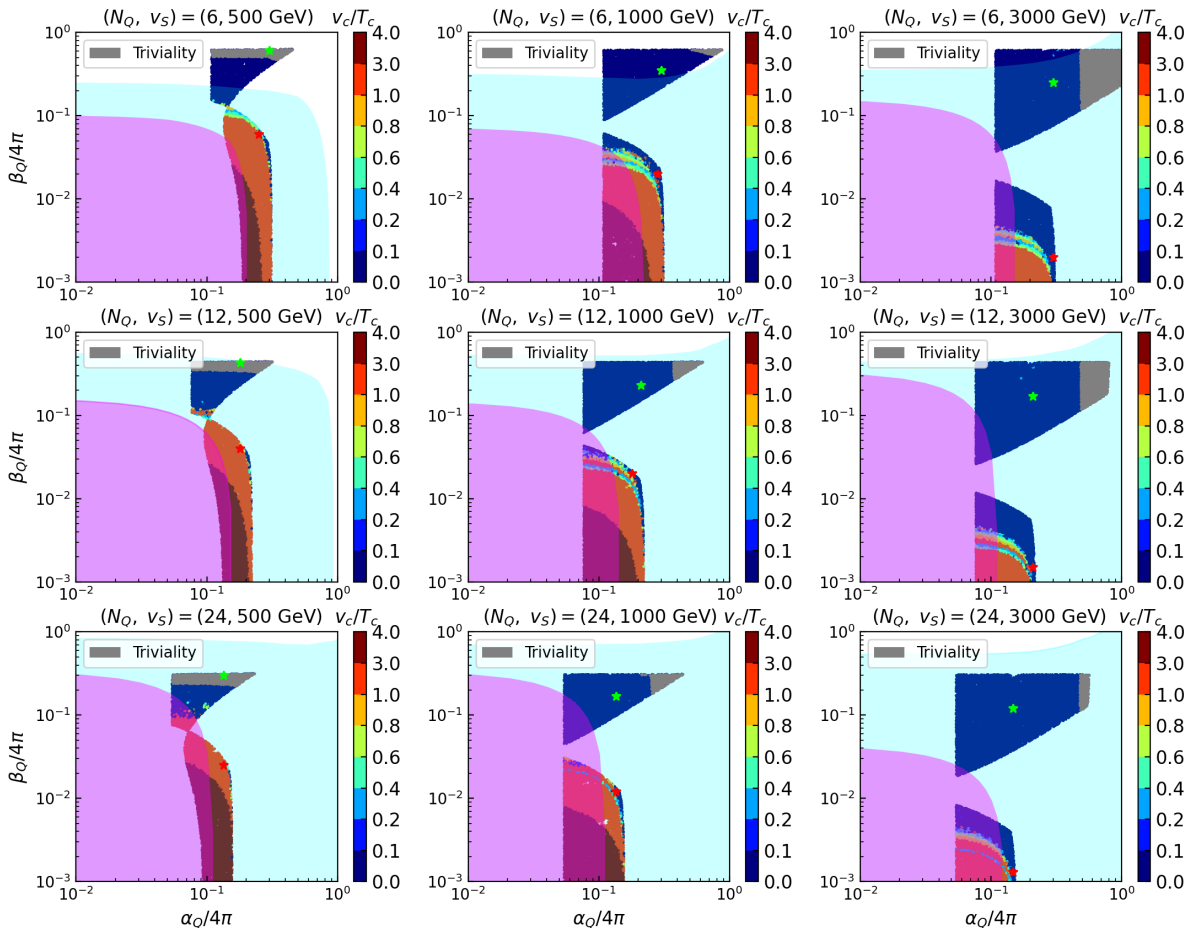


Figure 1. The dependence of the EWPT strength parameter v_c/T_c on the couplings (α_Q, β_Q) with different values of the multiplicity N_Q and the singlet VEV v_S . The green and red stars are the benchmark points (BPs) that correspond to the PRHM and light dilaton scenarios, respectively, which will be used in Fig. 3. The area colored in cyan represents the parameter space region that could be tested by DECIGO, while the magenta region is eliminated by the completion condition for the first order EWPT (4.8). The gray region is constrained by the triviality bound with $\Lambda_{\text{Lan}} < 10$ TeV.

interference region between the upper and lower islands. This option cannot be realized in cases with the large v_S .

In order to understand more about the EWPT dynamics, we show the relative difference between the critical and the nucleation temperature values $(T_c - T_n)/T_n$ in Fig. 2 for different values of the model free parameters.

Since this difference is significantly large, the first order EWPT in our analysis can be supercooling. In Fig. 2, it is shown that the relative difference $(T_c - T_n)/T_n$ is large for larger singlet VEV v_S , and/or smaller couplings (α_Q, β_Q) . As a consequence, the testable GWs can be produced even if the EWPT strength parameter v_c/T_c is smaller than unity. This is the reason why the wide parameter space region in Fig. 1 can be probed by GW experiments.

By considering the two BPs that correspond to the green (PRHM case) and red (light dilaton case) stars in Fig. 1, we show the GW amplitude $\Omega_{\text{GW}}h^2$ as functions of the frequency values. We conclude from Fig. 3 that our model may be tested at future space-based interferometers such as LISA [41], DECIGO [42], TianQin [103] and Taiji [104]. Even if the predicted GW spectrum cannot reach the sensitivity curves of the future GW observations, we may be able to extract the information of the GWs by using improved analysis methods [105, 106]. However,

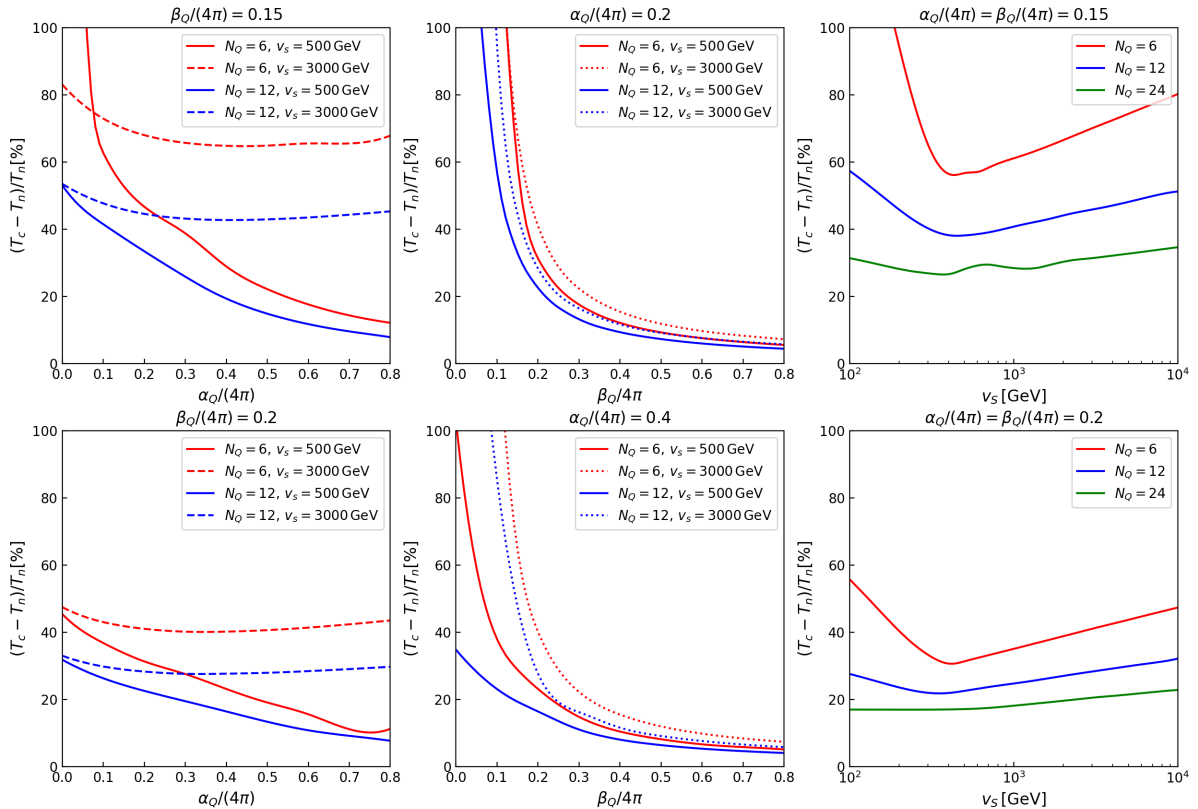


Figure 2. The relative difference between the critical and the nucleation temperature values in function of the couplings α_Q (left) β_Q (middle) and the singlet VEV v_S (right). The phase transition in our model is clearly supercooling.

we do not consider these methods in our analysis for the sake of simplicity.

As shown in Fig. 3, the peak height of the GW amplitude lowers as the value of β_Q gets smaller in general. Here, one has to mention that for small v_S values, the light dilaton scenario is most likely to be detectable than the PRHM one. The qualitative reason is as follows. The strength of the first order phase transition is generally related to the potential difference at the zero temperature between the symmetric vacuum $(H, s) = (0, 0)$ and the broken vacuum $(H, s) = (v, v_S)$. The potential difference is approximately given by

$$V_{\text{eff}}(0, 0) - V_{\text{eff}}(v, v_S) \simeq \frac{N_Q m_Q^4}{128\pi^2}, \quad (5.1)$$

where the loop corrections from the SM particles are neglected here. According to Eq. (5.1), the parameters N_Q , α_Q and β_Q should be small to make a high potential barrier, which means that the EWPT is strongly first order in the parameter space region with small N_Q , α_Q and β_Q .

Generally, in models with singlet scalar fields a non-trivial vacuum $(0, s \neq 0)$ can be preferred rather than the origin $(0, 0)$. If such vacuum exists, the strongly first order EWPT can be easily realized [23]. In order to avoid the existence of such non-trivial vacuum, the following condition should be satisfied

$$\lambda_S + \delta\lambda_S + \frac{3}{32\pi^2} N_Q \beta_Q^2 \left[\log \left(\frac{T^2}{\Lambda^2} \right) + 0.99 \right] > 0. \quad (5.2)$$

Since our model has a Z_2 symmetry $s \rightarrow -s$ even at the quantum level, the condition in Eq. (5.2) is always satisfied. Therefore, the approximation in Eq. (5.1) is meaningful in our model.

We note that the typical values of α and β we found are around 0.1 – 1 and 100 – 10000, respectively. It is well known that the bubble collision contribution can be dominant when

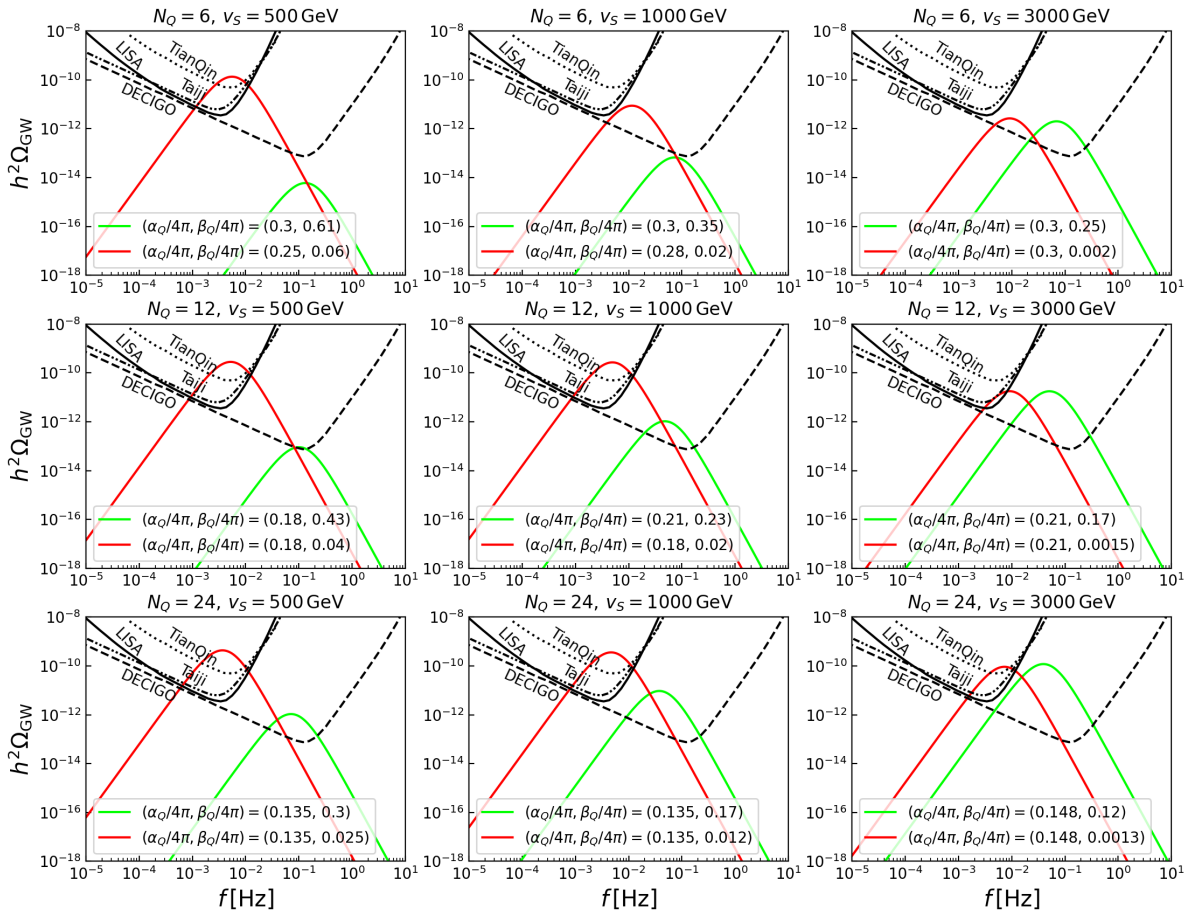


Figure 3. The predicted GW spectra for the two BPs with different values of the multiplicity N_Q and the singlet VEV v_s . The red and green lines correspond to the light dilaton scenario and the PRHM scenario, respectively, as shown as the green and red starts in Fig. 1. We also show the sensitivity curves of LISA [41], DECIGO [42], TianQin [103] and Taiji [104].

$\alpha \gg 1$ [99]. Our results indicate that the dominant source of the GWs in our scenario is the sound wave contribution.

As noted above, the parameter space region satisfying the condition in Eq. (1.2) may imply a large deviation in the cross section for the di-Higgs production from the SM prediction. To confirm this, we present the di-Higgs production cross section at the LHC and ILC in Fig. 4 and Fig. 5, respectively. These figures show the ratio of R_{LHC} and R_{ILC} as defined in Eq. (3.1) for different values of N_Q and v_s . These figures are produced by taking into account the different theoretical and experimental constraints that are mentioned above. According to Fig. 4 and Fig. 5, the large α_Q values are preferred to realize a large deviation in the cross section of the di-Higgs production from the SM prediction. As was mentioned earlier, for the light dilaton case, the R ratios cannot be large due to the constraints from the mixing angle and the completion condition for the phase transition. This means that we can distinguish the PRHM and the light dilaton scenarios by combining the measurement of the R_{LHC} and R_{ILC} with the GW observations. By comparing Fig. 4 with Fig. 5, the value of R_{ILC} is larger than R_{LHC} . One has to mention that the recent LHC negative searches for the di-Higgs signal established the upper bound on the di-Higgs production cross section $\sigma_{hh}^{\text{LHC}} < 112 \text{ fb}$ [64], which excludes significant regions in the parameter space, especially in the case with $v_s = 3 \text{ TeV}$. These regions are presented in Fig. 5 as the black dashed regions. Thus, it is expected that the ILC may impose more severe constraints on the parameter space region with a large deviation in the R ratios.

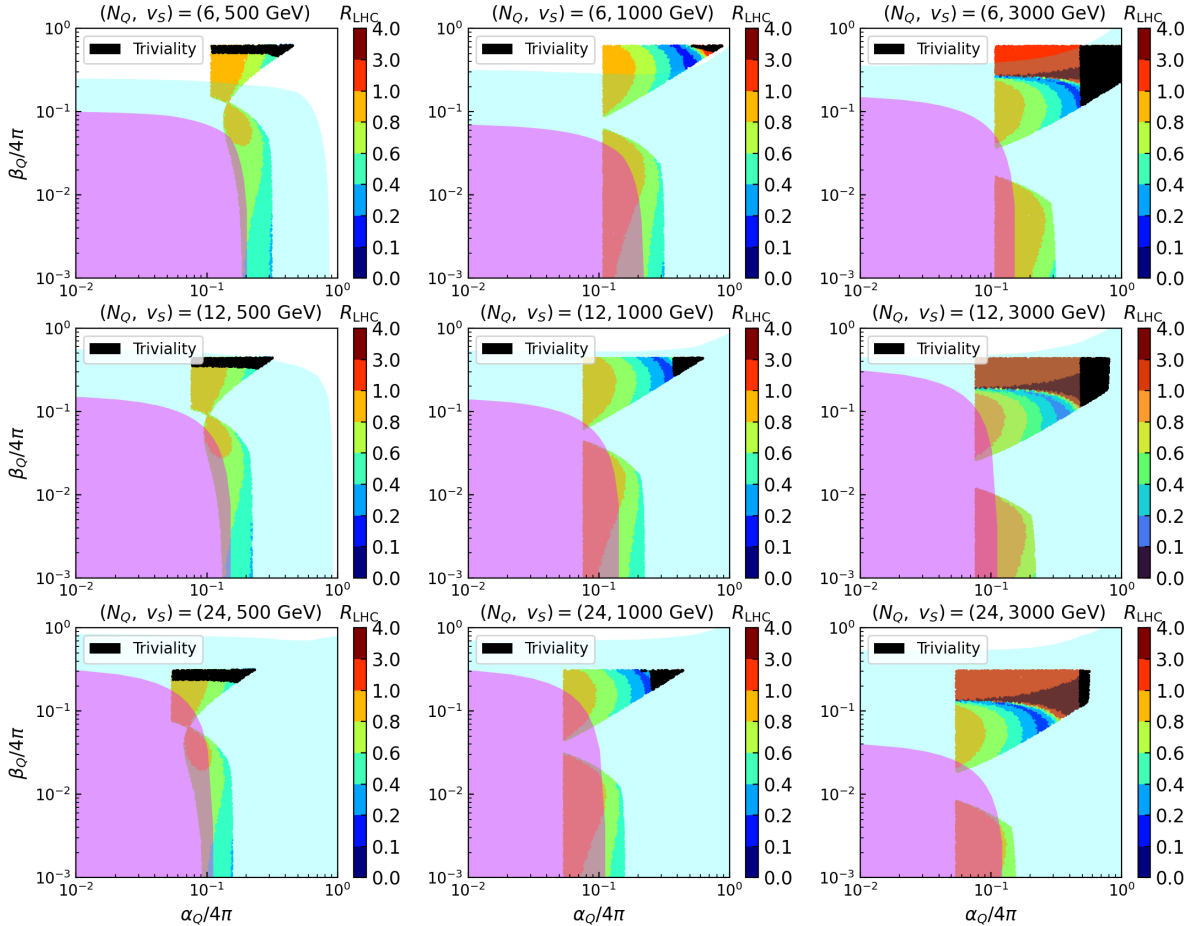


Figure 4. The parameter dependence for the value of R_{LHC} . The cyan region can be explored by the GW observations at the DECIGO. The magenta region is excluded by the completion condition for the phase transition in Eq (4.8). The large deviation in the cross section for the di-Higgs production prefers the large α_Q . The black region is constrained by the triviality bound with $\Lambda_{\text{Lan}} < 10$ TeV.

In Fig. 6, we show that the constraints on the model from current and future collider experiments such as the LHC, HL-LHC and ILC. The orange and gray regions can be explored by the LHC [64] and HL-LHC [65], respectively. The yellow regions are within the reach of the ILC with $\sqrt{s} = 500$ GeV [66], while the blue regions cannot be explored by the di-Higgs production measurement at the LHC, HL-LHC and ILC. On the other hand, the GW observations can be used to probe the models within the blue region.

Even if the PRHM scenario cannot be distinguished from the dilaton scenario by the di-Higgs production measurements, we can determine which scenario is preferred by combining collider and GW results. For instance, we focus on the two BPs with $N_Q = 12$ and $v_S = 3$ TeV shown in Fig. 2. The predicted GW spectra of these BPs has been shown in the panel with $N_Q = 12$ and $v_S = 3$ TeV in Fig. 3. One remarks that the positions of peak of the GWs are close. However, the GW peak position in the PRHM scenario is different from that in the light dilaton scenario. This implies that we are able to determine which scenario is preferred by observing the GW spectra even if a large cross section di-Higgs signal would not be observed at future collider experiments. Therefore, one can determine whether the PRHM scenario or the light dilaton scenario are realized by utilizing complementarity of collider experiments and GW observations.

We provide a commentary on the Landau pole scale in our scenario. It has been numerically confirmed that the typical Landau pole scale in our model is around $O(1)$ TeV when using the

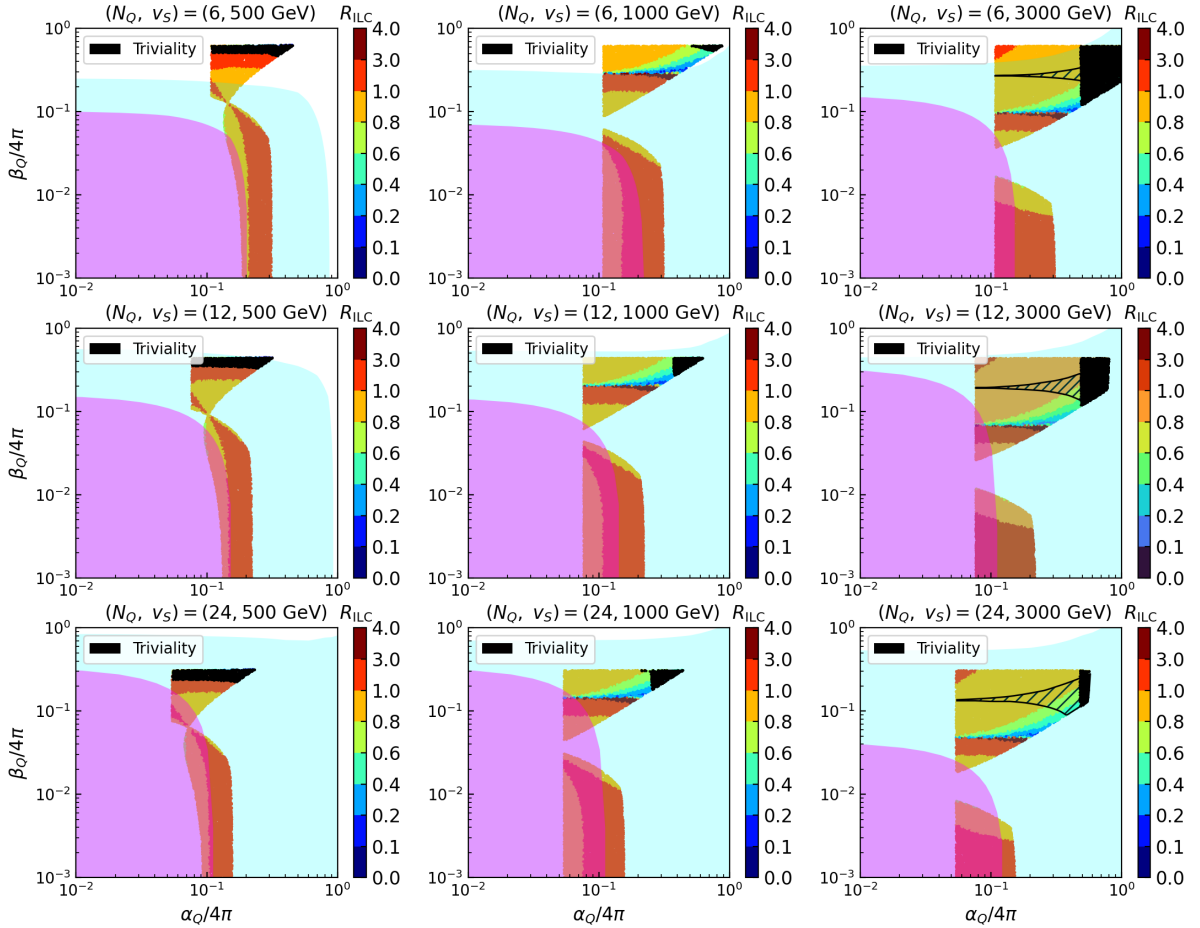


Figure 5. The parameter dependence for the value of R_{ILC} . The cyan region can be explored by the GW observations at the DECIGO. The magenta region is excluded by the completion condition for the phase transition in Eq. (4.8). The black shaded region is the current constraint on the di-Higgs production from the LHC results. The black region is constrained by the triviality bound with $\Lambda_{\text{Lan}} < 10$ TeV.

N_Q	$v_S = 500$ GeV	$v_S = 1$ TeV	$v_S = 3$ TeV
6	(R) 31.0 TeV (G) 7.05 TeV	(R) 19.8 TeV (G) 26.0 TeV	(R) 14.9 TeV (G) 53.0 TeV
12	(R) 34.0 TeV (G) 6.66 TeV	(R) 37.6 TeV (G) 40.3 TeV	(R) 17.4 TeV (G) 92.8 TeV
24	(R) 27.5 TeV (G) 6.19 TeV	(R) 29.7 TeV (G) 46.6 TeV	(R) 19.3 TeV (G) 96.9 TeV

Table 2. The Landau pole scale values with the mass dependent beta functions. Here, (R) and (G) denote the values for the BPs considered in Fig. 3.

beta functions outlined in Appendix A. In Table 2, the Landau pole scales for the two BPs considered in Fig. 3, with mass-dependent beta functions, are presented. The results in Table 2 indicate that the typical values of Λ_{Lan} in our model are around $O(10)$ TeV. This finding suggests that our phenomenological analyses satisfy perturbativity.

For the PRHM scenarios with $v_s = 500$, GeV, the Landau pole scale can be in the $O(1)$ TeV range. However, such BPs are constrained by the triviality bound with $\Lambda_{\text{Lan}} < 10$, TeV.

Before closing this section, we would like to comment on the possibility of projecting our results to other renormalizable new physics models. In this work, we considered a generic CSI model, where the quantum effects that trigger the EWSB lead to the EWPT dynamics and GWs discussed above. These quantum corrections lead to the same behavior whether they are a consequence of single/multiple field contributions that are just bosonic or bosonic and fermionic

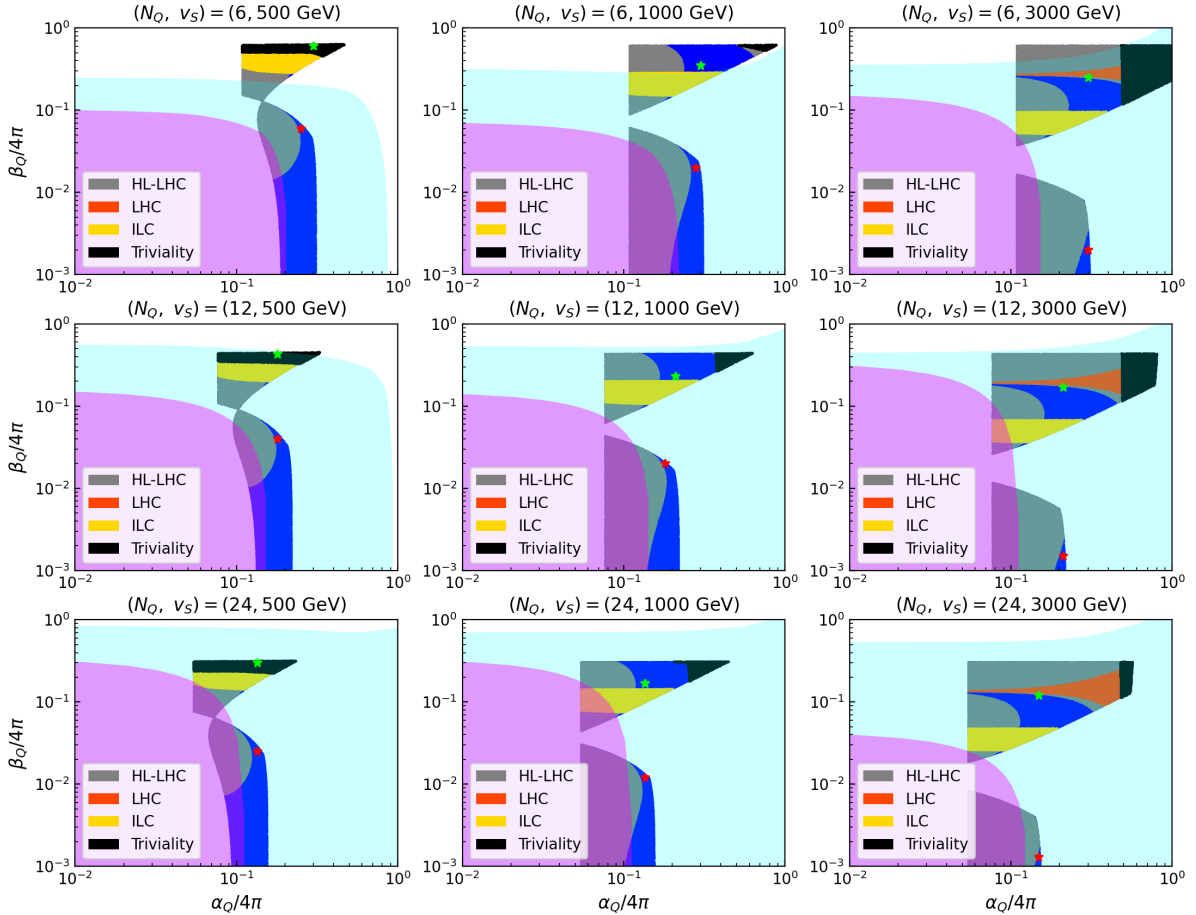


Figure 6. The parameter space region explored by the LHC, HL-LHC and ILC. The gray, orange and green regions are explored by HL-LHC, LHC and ILC, respectively. DECIGO can explore the cyan shaded region. The magenta region is constrained by the completion condition for the phase transition. The blue regions are the unexplored parameter space regions. The black region is constrained by the triviality bound with $\Lambda_{\text{Lan}} < 10 \text{ TeV}$.

contributions. However, in renormalizable new physics models, additional model-dependent theoretical and experimental constraints should be considered; and the viable parameter space is significantly affected. For instance, if such a new physics model suggests a DM candidate; and/or proposes a solution to the neutrino mass smallness problem, the new masses and couplings in the model would be severely constrained not only by the motivation requirements (DM relic density and/or neutrino mass smallness); but also by other constraints like lepton flavor violating processes, Higgs invisible and di-photon decays. For instance, in the current generic model, if the singlet Q is considered to be $U(1)_Y$ charged, a significant part of the parameter space α_Q , β_Q , N_Q and v_S would be excluded by the bound from $h \rightarrow \gamma\gamma$. Therefore, one expects that the parameter space regions where the light dilation or PRHM scenarios can be realized are in general narrowed down when specific new physics models are considered.

6 Conclusion

In this work, we have investigated the possibility of detectable GWs that are produced during a strongly first order EWPT, within a class of models with the CSI. In order to get model independent results, we have considered the SM extended by a real scalar singlet to assist the EWSB, and an additional scalar field with multiplicity N_Q , and couplings α_Q and β_Q that

accounts for the RCs. By scanning over the model free parameters (N_Q , α_Q , β_Q and v_S), the impact of the RCs on the EWPT and GW observables have been estimated. Especially, we have focused on the difference between the light dilaton and PRHM scenarios. We have analyzed the properties of the GWs from a strongly first order EWPT by considering a generic model with the CSI. We have shown that peaked GW spectrum might be detected at future space-based interferometers such as the DECIGO and other GW observations even if the condition $v_c/T_c > 1$ is not satisfied. As a result, the wide parameter space region in the CSI model may be tested by utilizing the GW observations.

Also, we have analyzed the cross section in the di-Higgs production processes at the LHC and ILC. As we have shown, the cross section can be more than three times larger than the SM prediction in the PRHM scenario. As shown in Fig. 6, the parameter regions with such large deviation in the di-Higgs production process can be explored at the LHC, HL-LHC and ILC. In addition, we have shown that GW observations are useful to distinguish the light dilaton scenario from the PRHM scenario even if collider experiments cannot observe the di-Higgs production signal. This fact indicates that we may be able to determine whether the light dilaton scenario or the PRHM scenario is preferred by utilizing complementary of collider experiments and GW observations.

Acknowledgements

A. A. was funded by the University of Sharjah under the research projects No 21021430107 “*Hunting for New Physics at Colliders*” and No 23021430135 “*Terascale Physics: Colliders vs Cosmology*”. S. K. was supported by the JSPS KAKENHI Grant No. 20H00160, No. 202F21324 and No. 203K17691. M. T. was supported by JSPS KAKENHI Grant No. JP21J10645. M. T. would like to thank Sharjah university (IAESTE exchange program, HEP group, RISE and VCRGS) for the financial support and the warm hospitality.

A Renormalization Group Equations

In this appendix, the renormalization group equations for the couplings in our model are discussed. The beta functions for each coupling in our model at one-loop level are given by

$$\begin{aligned}
16\pi^2\beta_{g'} &= \frac{41}{6}g'^3, 16\pi^2\beta_g = -\frac{19}{6}g^3, 16\pi^2\beta_{g_3} = -7g_3^3, \\
16\pi^2\beta_{y_t} &= y_t \left(-8g_3^2 - \frac{9}{4}g^2 - \frac{17}{12}g'^2 + \frac{9}{2}y_t^2 \right), \\
16\pi^2\beta_{\lambda_h} &= 4\lambda_h^2 + 3N_Q\alpha_Q^2 + 3\omega^2 + \frac{27}{4}g^4 + \frac{9}{2}g^2g'^2 + \frac{9}{4}g'^4 - 36y_t^4 - \lambda_h(9g^2 + 3g'^2 - 12y_t^2), \\
16\pi^2\beta_{\lambda_s} &= 3\lambda_s^2 + 3N_Q\beta_Q^2 + 12\omega^2, 16\pi^2\beta_{\lambda_Q} = \frac{N_Q+8}{3}\lambda_Q^2 + 3\beta_Q^2 + 12\alpha_Q^2, \\
16\pi^2\beta_\omega &= 4\omega^2 + \omega\lambda_s + 2\lambda_h\omega + N_Q\alpha_Q\beta_Q + 6\omega y_t^2 - \frac{9}{2}\omega g^2 - \frac{3}{2}\omega g'^2, \\
16\pi^2\beta_{\alpha_Q} &= 4\alpha_Q^2 + \frac{N_Q+2}{3}\alpha_Q\lambda_Q + 2\alpha_Q\lambda_h + \omega\beta_Q + 6\alpha_Q y_t^2 - \frac{9}{2}\alpha_Q g^2 - \frac{3}{2}\alpha_Q g'^2, \\
16\pi^2\beta_{\beta_Q} &= 4\beta_Q^2 + \frac{N_Q+2}{3}\lambda_Q\beta_Q + \lambda_s\beta_Q + 4\omega\alpha_Q,
\end{aligned} \tag{A.1}$$

where g' , g and g_3 are gauge couplings for $U(1)_Y$, $SU(2)_L$ and $SU(3)_C$ gauge groups, respectively. Also, y_t is the Yukawa coupling for top quarks. It is confirmed that these equations are consistent with the previous work if we take $N_Q = 1$ [107].

References

- [1] G. Aad et al. [ATLAS], Phys. Lett. B **716**, 1-29 (2012) [arXiv:1207.7214 [hep-ex]]. S. Chatrchyan *et al.* [CMS], Phys. Lett. B **716** (2012), 30-61 [arXiv:1207.7235 [hep-ex]].
- [2] W. A. Bardeen, FERMILAB-CONF-95-391-T.
- [3] J. S. Lee and A. Pilaftsis, Phys. Rev. D **86**, 035004 (2012) [arXiv:1201.4891 [hep-ph]].
- [4] C. Englert, J. Jaeckel, V. V. Khoze and M. Spannowsky, JHEP **04**, 060 (2013) [arXiv:1301.4224 [hep-ph]].
- [5] J. Guo and Z. Kang, Nucl. Phys. B **898**, 415-430 (2015) [arXiv:1401.5609 [hep-ph]].
- [6] K. Endo and Y. Sumino, JHEP **05**, 030 (2015) [arXiv:1503.02819 [hep-ph]].
- [7] K. Hashino, S. Kanemura and Y. Orikasa, Phys. Lett. B **752**, 217-220 (2016) [arXiv:1508.03245 [hep-ph]].
- [8] K. Hashino, M. Kakizaki, S. Kanemura and T. Matsui, Phys. Rev. D **94**, 015005 (2016) [arXiv:1604.02069 [hep-ph]].
- [9] A. Ahriche, K. L. McDonald and S. Nasri, JHEP **06**, 182 (2016) [arXiv:1604.05569 [hep-ph]].
- [10] A. Ahriche, A. Manning, K. L. McDonald and S. Nasri, Phys. Rev. D **94**, no.5, 053005 (2016) [arXiv:1604.05995 [hep-ph]].
- [11] K. Lane and E. Pilon, Phys. Rev. D **101**, no.5, 055032 (2020) [arXiv:1909.02111 [hep-ph]].
- [12] S. Kanemura and M. Tanaka, Phys. Lett. B **809**, 135711 (2020) [arXiv:2005.05250 [hep-ph]].
- [13] J. Braathen, S. Kanemura and M. Shimoda, JHEP **03**, 297 (2021) [arXiv:2011.07580 [hep-ph]].
- [14] A. Ahriche, Nucl. Phys. B **982** (2022), 115896 [arXiv:2110.10301 [hep-ph]].
- [15] R. Soualah and A. Ahriche, Phys. Rev. D **105** (2022) no.5, 055017 [arXiv:2111.01121 [hep-ph]].
- [16] E. J. Eichten and K. Lane, Phys. Rev. D **107**, no.7, 075038 (2023) [arXiv:2209.06632 [hep-ph]].
- [17] S. R. Coleman and E. J. Weinberg, Phys. Rev. D **7**, 1888-1910 (1973).
- [18] E. Gildener and S. Weinberg, Phys. Rev. D **13** (1976), 3333.
- [19] N. Aghanim *et al.* [Planck], Astron. Astrophys. **641** (2020), A6 [erratum: Astron. Astrophys. **652** (2021), C4] [arXiv:1807.06209 [astro-ph.CO]].
- [20] A. D. Sakharov, Pisma Zh. Eksp. Teor. Fiz. **5** (1967), 32-35
- [21] V. A. Kuzmin, V. A. Rubakov and M. E. Shaposhnikov, Phys. Lett. B **155** (1985), 36
- [22] A. I. Bochkarev and M. E. Shaposhnikov, Mod. Phys. Lett. A **2** (1987), 417. A. I. Bochkarev, S. V. Kuzmin and M. E. Shaposhnikov, Phys. Rev. D **43** (1991), 369-374
- [23] A. Ahriche, Phys. Rev. D **75** (2007), 083522 [arXiv:hep-ph/0701192 [hep-ph]].
- [24] A. Ahriche, T. A. Chowdhury and S. Nasri, JHEP **11** (2014), 096 [arXiv:1409.4086 [hep-ph]].
- [25] K. Fuyuto and E. Senaha, Phys. Rev. D **90**, no.1, 015015 (2014) [arXiv:1406.0433 [hep-ph]].
- [26] S. Kanemura and M. Tanaka, Phys. Rev. D **106**, no.3, 035012 (2022) [arXiv:2201.04791 [hep-ph]].
- [27] S. Kanemura, Y. Okada and E. Senaha, Phys. Lett. B **606**, 361-366 (2005) [arXiv:hep-ph/0411354 [hep-ph]].
- [28] M. A. Shifman, A. I. Vainshtein, M. B. Voloshin and V. I. Zakharov, Sov. J. Nucl. Phys. **30**, 711-716 (1979) ITEP-42-1979.
- [29] S. Kanemura, S. Kiyoura, Y. Okada, E. Senaha and C. P. Yuan, Phys. Lett. B **558**, 157-164 (2003) [arXiv:hep-ph/0211308 [hep-ph]].
- [30] S. Kanemura, Y. Okada, E. Senaha and C. P. Yuan, Phys. Rev. D **70**, 115002 (2004) [arXiv:hep-ph/0408364 [hep-ph]].
- [31] A. Arhrib, R. Benbrik and N. Gaur, Phys. Rev. D **85**, 095021 (2012) [arXiv:1201.2644 [hep-ph]].

- [32] S. Kanemura, M. Kikuchi, K. Mawatari, K. Sakurai and K. Yagyu, Nucl. Phys. B **949**, 114791 (2019) [arXiv:1906.10070 [hep-ph]].
- [33] S. Kanemura, M. Kikuchi, K. Mawatari, K. Sakurai and K. Yagyu, Comput. Phys. Commun. **257**, 107512 (2020) [arXiv:1910.12769 [hep-ph]].
- [34] G. Degrandi and P. Slavich, [arXiv:2307.02476 [hep-ph]].
- [35] M. Aiko, J. Braathen and S. Kanemura, [arXiv:2307.14976 [hep-ph]].
- [36] A. Kosowsky, M. S. Turner and R. Watkins, Phys. Rev. D **45** (1992), 4514-4535.
- [37] M. Kamionkowski, A. Kosowsky and M. S. Turner, Phys. Rev. D **49** (1994), 2837-2851 [arXiv:astro-ph/9310044 [astro-ph]].
- [38] P. Schwaller, Phys. Rev. Lett. **115** (2015) no.18, 181101 [arXiv:1504.07263 [hep-ph]].
- [39] A. Kosowsky, M. S. Turner and R. Watkins, Phys. Rev. Lett. **69** (1992), 2026-2029.
- [40] C. Grojean and G. Servant, Phys. Rev. D **75**, 043507 (2007) [hep-ph/0607107].
- [41] P. Amaro-Seoane *et al.* [LISA], [arXiv:1702.00786 [astro-ph.IM]].
- [42] S. Kawamura, T. Nakamura, M. Ando, N. Seto, K. Tsubono, K. Numata, R. Takahashi, S. Nagano, T. Ishikawa and M. Musha, *et al.* Class. Quant. Grav. **23** (2006), S125-S132.
- [43] M. Kakizaki, S. Kanemura and T. Matsui, Phys. Rev. D **92**, no.11, 115007 (2015) [arXiv:1509.08394 [hep-ph]].
- [44] P. Huang, A. J. Long and L. T. Wang, Phys. Rev. D **94**, no.7, 075008 (2016) [arXiv:1608.06619 [hep-ph]].
- [45] K. Hashino, M. Kakizaki, S. Kanemura, P. Ko and T. Matsui, Phys. Lett. B **766**, 49-54 (2017) [arXiv:1609.00297 [hep-ph]].
- [46] K. Hashino, M. Kakizaki, S. Kanemura, P. Ko and T. Matsui, JHEP **06**, 088 (2018) [arXiv:1802.02947 [hep-ph]].
- [47] V. Brdar, A. J. Helmboldt and J. Kubo, JCAP **02**, 021 (2019) [arXiv:1810.12306 [hep-ph]].
- [48] V. Brdar, A. J. Helmboldt and M. Lindner, JHEP **12**, 158 (2019) [arXiv:1910.13460 [hep-ph]].
- [49] A. Salvio, JCAP **04**, 051 (2023) [arXiv:2302.10212 [hep-ph]].
- [50] A. Salvio, [arXiv:2307.04694 [hep-ph]].
- [51] A. Farzinnia and J. Ren, Phys. Rev. D **90** (2014) no.7, 075012 [arXiv:1408.3533 [hep-ph]].
- [52] A. Mohamadnejad, Eur. Phys. J. C **80** (2020) no.3, 197 [arXiv:1907.08899 [hep-ph]].
- [53] J. Kubo and M. Yamada, PTEP **2015** (2015) no.9, 093B01 [arXiv:1506.06460 [hep-ph]].
- [54] F. Sannino and J. Virkajervi, Phys. Rev. D **92** (2015) no.4, 045015 [arXiv:1505.05872 [hep-ph]].
- [55] M. Kierkla, A. Karam and B. Swiezewska, JHEP **03**, 007 (2023) [arXiv:2210.07075 [astro-ph.CO]].
- [56] K. Hashino, S. Kanemura and T. Takahashi, Phys. Lett. B **833**, 137261 (2022) [arXiv:2111.13099 [hep-ph]].
- [57] K. Hashino, S. Kanemura, T. Takahashi and M. Tanaka, Phys. Lett. B **838**, 137688 (2023) [arXiv:2211.16225 [hep-ph]].
- [58] <https://hsc.mtk.nao.ac.jp/ssp/>.
- [59] <http://ogle.astrouw.edu.pl>.
- [60] <http://www-ir.ess.sci.osaka-u.ac.jp/prime/index.html>
- [61] <https://roman.gsfc.nasa.gov>
- [62] L. Alexander-Nunneley and A. Pilaftsis, JHEP **09**, 021 (2010) [arXiv:1006.5916 [hep-ph]].
- [63] S. Kanemura, E. Senaha, T. Shindou and T. Yamada, JHEP **05**, 066 (2013) [arXiv:1211.5883 [hep-ph]].
- [64] A. Tumasyan *et al.* [CMS], Nature **607**, no.7917, 60-68 (2022) [arXiv:2207.00043 [hep-ex]].

- [65] M. Cepeda, S. Gori, P. Ilten, M. Kado, F. Riva, R. Abdul Khalek, A. Aboubrahim, J. Alimena, S. Alioli and A. Alves, *et al.* CERN Yellow Rep. Monogr. **7**, 221-584 (2019) [arXiv:1902.00134 [hep-ph]].
- [66] P. Bambade, T. Barklow, T. Behnke, M. Berggren, J. Brau, P. Burrows, D. Denisov, A. Faus-Golfe, B. Foster and K. Fujii, *et al.* [arXiv:1903.01629 [hep-ex]].
- [67] A. Arhrib, R. Benbrik, C. H. Chen, R. Guedes and R. Santos, JHEP **08**, 035 (2009) [arXiv:0906.0387 [hep-ph]].
- [68] M. J. Dolan, C. Englert and M. Spannowsky, Phys. Rev. D **87**, no.5, 055002 (2013) [arXiv:1210.8166 [hep-ph]].
- [69] S. Kanemura, M. Kikuchi and K. Yagyu, Nucl. Phys. B **917**, 154-177 (2017) [arXiv:1608.01582 [hep-ph]].
- [70] S. Dawson and M. Sullivan, Phys. Rev. D **97**, no.1, 015022 (2018) [arXiv:1711.06683 [hep-ph]].
- [71] M. Carena, Z. Liu and M. Riembau, Phys. Rev. D **97**, no.9, 095032 (2018) [arXiv:1801.00794 [hep-ph]].
- [72] F. Arco, S. Heinemeyer and M. J. Herrero, Eur. Phys. J. C **81**, no.10, 913 (2021) [arXiv:2106.11105 [hep-ph]].
- [73] H. Abouabid, A. Arhrib, D. Azevedo, J. E. Falaki, P. M. Ferreira, M. Mühlleitner and R. Santos, JHEP **09**, 011 (2022) [arXiv:2112.12515 [hep-ph]].
- [74] S. Iguro, T. Kitahara, Y. Omura and H. Zhang, Phys. Rev. D **107**, no.7, 075017 (2023) [arXiv:2211.00011 [hep-ph]].
- [75] G. Aad *et al.* [ATLAS and CMS], JHEP **08** (2016), 045 [arXiv:1606.02266 [hep-ex]].
- [76] M. Lindner, Z. Phys. C **31**, 295 (1986)
- [77] S. Kanemura and Y. Mura, [arXiv:2310.15622 [hep-ph]].
- [78] C. Grojean, G. Servant and J. D. Wells, Phys. Rev. D **71**, 036001 (2005) [arXiv:hep-ph/0407019 [hep-ph]].
- [79] A. Noble and M. Perelstein, Phys. Rev. D **78** (2008), 063518 [arXiv:0711.3018 [hep-ph]].
- [80] A. Ahriche, A. Arhrib and S. Nasri, Phys. Lett. B **743** (2015), 279-283 [arXiv:1407.5283 [hep-ph]].
- [81] M. Spira, [arXiv:hep-ph/9510347 [hep-ph]].
- [82] G. Aad *et al.* [ATLAS], Phys. Rev. Lett. **125** (2020) no.5, 051801 [arXiv:2002.12223 [hep-ex]].
- [83] G. Aad *et al.* [ATLAS], Eur. Phys. J. C **81** (2021) no.4, 332 [arXiv:2009.14791 [hep-ex]].
- [84] A. Tumasyan *et al.* [CMS], [arXiv:2109.06055 [hep-ex]].
- [85] G. Aad *et al.* [ATLAS], ATLAS-CONF-2021-030.
- [86] G. Aad *et al.* [ATLAS], ATLAS-CONF-2021-035.
- [87] G. Aad *et al.* [ATLAS], ATLAS-CONF-2021-016.
- [88] D. Croon, O. Gould, P. Schicho, T. V. I. Tenkanen and G. White, JHEP **04**, 055 (2021) [arXiv:2009.10080 [hep-ph]].
- [89] J. Löfgren, M. J. Ramsey-Musolf, P. Schicho and T. V. I. Tenkanen, Phys. Rev. Lett. **130**, no.25, 251801 (2023) [arXiv:2112.05472 [hep-ph]].
- [90] P. Schicho, T. Tenkanen, V.I. and G. White, JHEP **11**, 047 (2022) [arXiv:2203.04284 [hep-ph]].
- [91] L. Dolan and R. Jackiw, Phys. Rev. D **9**, 3320 (1974). Weinberg, Phys. Rev. D **9**, 3357 (1974).
- [92] M. E. Carrington, Phys. Rev. D **45**, 2933 (1992).
- [93] D. J. Gross, R. D. Pisarski and L. G. Yaffe, Rev. Mod. Phys. **53** (1981), 43.
- [94] A. Ahriche, K. Hashino, S. Kanemura and S. Nasri, Phys. Lett. B **789** (2019), 119-126 [arXiv:1809.09883 [hep-ph]].
- [95] A. D. Linde, Nucl. Phys. B **216**, 421 (1983) [erratum: Nucl. Phys. B **223**, 544 (1983)].

- [96] C. L. Wainwright, *Comput. Phys. Commun.* **183**, 2006-2013 (2012) [arXiv:1109.4189 [hep-ph]].
- [97] S. J. Huber and T. Konstandin, *JCAP* **09** (2008), 022 [arXiv:0806.1828 [hep-ph]].
- [98] C. Caprini and R. Durrer, *Phys. Rev. D* **74** (2006), 063521 [arXiv:astro-ph/0603476 [astro-ph]].
- [99] C. Caprini, M. Hindmarsh, S. Huber, T. Konstandin, J. Kozaczuk, G. Nardini, J. M. No, A. Petiteau, P. Schwaller and G. Servant, *et al.* *JCAP* **04** (2016), 001. [arXiv:1512.06239 [astro-ph.CO]].
- [100] J. R. Espinosa, T. Konstandin, J. M. No and G. Servant, *JCAP* **06**, 028 (2010) [arXiv:1004.4187 [hep-ph]].
- [101] M. O. Khojali, A. Abdalgabar, A. Ahriche and A. S. Cornell, *Phys. Rev. D* **106** (2022) no.9, 095039 [arXiv:2206.06211 [hep-ph]].
- [102] N. Baouche, A. Ahriche, G. Faisel and S. Nasri, *Phys. Rev. D* **104** (2021) no.7, 075022 [arXiv:2105.14387 [hep-ph]].
- [103] J. Luo *et al.* [TianQin], *Class. Quant. Grav.* **33**, no.3, 035010 (2016) [arXiv:1512.02076 [astro-ph.IM]].
- [104] W. H. Ruan, Z. K. Guo, R. G. Cai and Y. Z. Zhang, *Int. J. Mod. Phys. A* **35**, no.17, 2050075 (2020) [arXiv:1807.09495 [gr-qc]].
- [105] K. Hashino, R. Jinno, M. Kakizaki, S. Kanemura, T. Takahashi and M. Takimoto, *Phys. Rev. D* **99**, no.7, 075011 (2019) [arXiv:1809.04994 [hep-ph]].
- [106] J. M. Cline, A. Friedlander, D. M. He, K. Kainulainen, B. Laurent and D. Tucker-Smith, *Phys. Rev. D* **103**, no.12, 123529 (2021) [arXiv:2102.12490 [hep-ph]].
- [107] A. Abada and S. Nasri, *Phys. Rev. D* **88**, no.1, 016006 (2013) [arXiv:1304.3917 [hep-ph]].